Wear 580-581 (2025) 206305

Contents lists available at ScienceDirect

Wear

journal homepage: www.elsevier.com/locate/wear

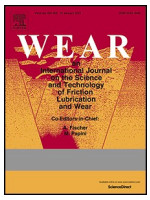

Load-dependent sliding behavior of WSe_{2-x} solid lubricant coating

Yue Wang [a,*], Himanshu Rai [a], Tomas Polcar [a,b,**]

[a] Advanced Materials Group, Faculty of Electrical Engineering, Czech Technical University in Prague, Technicka 4, Prague 6, 16000, Czech Republic
[b] School of Engineering, University of Southampton, Highfield, SO17 1BJ, Southampton, UK

A B S T R A C T

Transition-metal dichalcogenides (TMDs) are commonly used as solid lubricants in various environments. Molybdenum disulfide is the most studied and applied TMD solid lubricant, but other members may have similar or even better sliding properties. Tungsten diselenide is one of the materials that has rarely been investigated in terms of tribological properties. This paper provides a comprehensive tribological characterization of substoichiometric tungsten diselenide and molybdenum disulfide coatings deposited by magnetron sputtering. We focused on tribological properties at a macroscopic scale, particularly friction and wear dependence on applied load; however, a nanoscale frictional assessment of worn surfaces was performed as well to identify the major wear mechanisms. Substoichiometric tungsten diselenide outperformed traditional molybdenum disulfide, exhibiting much lower friction in humid air, suggesting lower coating sensitivity to the humid atmosphere. Moreover, a combination of nanotribological experiments in the wear tracks with sliding under different environmental conditions suggests that the key factor causing frictional load-dependence (deviation from Amonton's law) is frictional heating of the surface.

1. Introduction

Friction and wear cause substantial energy loss and material degradation and ultimately contribute to the mechanical failure of various engineering components. Solid lubricants possess exceptional physical and chemical properties, allowing them to reduce friction and wear in harsh conditions such as wide temperature ranges or various sliding speeds, making them potentially more efficient than liquid lubricants [1–3]. However, the challenge remains to identify optimum solid lubricants that can consistently and effectively minimize friction and wear in various sliding environments.

Transition-metal dichalcogenides (TMDs) stand out because of their layered structure and weak van der Waals bonding between the layers. Their structure facilitates interlayer shear, resulting in exceptionally low frictional properties of TMDs in vacuum [4]. However, when applied in industrial settings, TMD-based solid lubricant coatings often face environmental degradation. Water and oxygen molecules in the atmosphere play a detrimental role; water molecules are absorbed between TMDs layers, reducing the lubrication function at room temperature, and atmospheric oxygen leads to rapid oxidation [5,6]. Molybdenum disulfide, the most extensively studied TMD material, oxidizes at relatively low temperatures (approximately 300 °C) and exhibits a much higher coefficient of friction in ambient environments compared to vacuum [7,8]. To overcome the limitations of MoS_2, alternative TMD materials with a similar structure have been studied, such as WS_2 and $MoSe_2$. Replacement of molybdenum with tungsten enhances the oxidation-resistance of TMDs; it has been reported that tungsten disulfide can maintain its low coefficient of friction up to 500 °C [9]. Meanwhile, molybdenum diselenide is a better choice for a humid environment, providing a lower coefficient of friction than that of MoS_2; the reduction of friction can reach 50 % [10].

Considering properties of WS_2 and $MoSe_2$, tungsten diselenide, another member of the TMD family with a lamellar structure, is a promising choice with the potential to resist environmental attacks. The nanofriction characterization on WSe_2 monolayers in ambient air showed the lowest friction when compared to other tested TMDs flakes [11]. Some studies explored tungsten diselenide applied as a solid lubricant coating. Dominguez-Meister [12] and Evaristo [13] developed tungsten diselenide-based coating with a coefficient of friction as low as 0.08, which was lower than other TMD materials like MoS_2 and WS_2. Yet, the properties of WSe_2 as a solid lubricant are still almost unknown, particularly when compared to the most studied solid lubricant, MoS_2.

In this work, a comprehensive tribological characterization consisting of macroscale and nanoscale tribological tests was conducted on tungsten diselenide coatings deposited by magnetron sputtering and compared to MoS_2 reference films to investigate their tribological behavior. Macroscale tribological tests were conducted under various normal loads, while load-dependence nanotribological tests were performed on the wear tracks. Our results indicate that the WSe_{2-x} coating exhibits superior tribological performance in ambient environments

* Corresponding author.
** Corresponding author. School of Engineering, University of Southampton, Highfield, SO17 1BJ, Southampton, UK.
E-mail addresses: wangyue@fel.cvut.cz (Y. Wang), t.polcar@soton.ac.uk (T. Polcar).

https://doi.org/10.1016/j.wear.2025.206305
Received 28 June 2025; Received in revised form 11 August 2025; Accepted 22 August 2025
Available online 23 August 2025

compared to MoS_2 and displays load-adaptive sliding behavior. It is worth noting that the majority of sputtered TMDs are deficient in chalcogenide due to resputtering [14,15], but they are traditionally referred to as disulfides or diselenides.

2. Experiment section

2.1. Sample preparation

WSe_{2-x} and MoS_2 coatings were deposited by an AJA magnetron sputtering system with a 150 W DC power supply using pure WSe_2 and MoS_2 targets. Polished steel samples (WNr. 1.2379 steel), with a hardness of about 9 GPa, were selected as the substrates for coatings. Before the deposition, the substrate was sputter-cleaned under 50 W RF power for 30 min. A pure Cr layer (~150 nm) was deposited between the coating and substrate to improve adhesion. The deposition parameters are shown in Table 1. The coating thickness was measured by Zygo NewView 8000 profilometer.

2.2. Structure characterization

The coatings' morphology was characterized by SEM (MIRA3 XMU). Energy dispersive spectroscopy (EDS) determined the chemical composition. X-ray diffraction (Rigaku 3; Cu Kα) revealed the structure, whereas X-ray photoelectron spectroscopy was employed to identify chemical states; the samples were ion-etched for 5 min to remove surface contamination. The hardness and Young's modulus were measured by nanoindentation. After tribological testing, the wear tracks and ball scars were characterized by Raman (Horiba Xplora) with 532 nm laser excitation, and the data were compared with spectra taken from virgin samples. The morphologies of the wear tracks were characterized by a 3D White light optical profilometer (Zygo NV7200).

2.3. Macroscale tribological testing

Tribological tests were carried out using a Bruker UMT-2 tribometer in reciprocating mode at 1 Hz, with a stroke length of 3 mm. The test duration was 1000 s. The normal load was set to 1, 3, 5, 7, and 10 N, 10 mm AISI440C ball was used as a counterpart. The corresponding Hertz contact pressure is shown in Fig. S1. The steady-state coefficient of friction was obtained by taking an average after 300 laps of testing to avoid the running-in effect. The wear rate was calculated according to the following equation [16]:

$$K = \frac{V}{FL} \quad \text{Equation (1)}$$

Where V is the worn volume (mm^3), F is the normal load (N), and L is the sliding distance (m). All macroscale experiments were carried out in an ambient environment: 25 °C and relative air humidity of 40 %.

2.4. Nanotribological characterization

Nanotribological characterization of coatings and wear tracks was performed by scanning probe microscope (Bruker, Dimension ICON-SPM) in contact mode in an ambient environment. Surface topographies and friction maps were carried out on a 2 μm × 2 μm area. A DLC-coated AFM probe (ContDLC, BudgetSensors, Bulgaria), and normal loads were set to increment from 20 nN to 70 nN following the procedure in Refs. [17,18]. The lateral and normal spring constants of the cantilever were calibrated following the methods proposed by Sader [19] and Green et al. [20]. Calibration of lateral and normal forces was performed using the beam geometry method [21,22]. All AFM measurements were conducted in contact mode under consistent ambient conditions.

3. Experimental results

3.1. Coating characterization

The chemical composition of coatings was characterized by EDX, as shown in Table 2. The corresponding morphologies of each coating are shown in Fig. S2. Relatively high oxygen content in the as-deposited coatings is typical for such deposition processes and originates from residual atmosphere and from targets, which are porous and prone to surface oxidation. The WSe_{2-x} coating exhibited a significant deviation from stoichiometry, with a Se/W atomic ratio of 0.92, consistent with previous studies [23]. The loss of selenium in the deposition of WSe_{2-x} coating is likely the result of the resputtering effect caused by heavy tungsten atoms [24]. MoS_2 exhibits an S/Mo ratio of 1.91, which is close to stoichiometric. The WSe_{2-x} coating showed higher hardness (3.5 GPa) and Young's modulus (87.7 GPa) compared to the MoS_2 coating (0.5 and 25.4 GPa, respectively).

X-ray diffraction spectra are shown in Fig. 1 (a). In the case of MoS_2, the diffraction peaks of (002) and (100) at 14.1° and 33.5° belong to 2H-MoS_2 [24]. A small peak at 59.2° refers to (110) in 2H-MoS_2 [25]. Long asymmetric tail of (100) peak towards higher 2θ suggests turbostrating stacking of 10 L planes, a typical feature of sputtered MoS_2 coatings [26]. WSe_{2-x} pattern shows a peak located at 13.8°, which fits well (002) reflections of 2H-WSe_2 [27] A large, broad peak located at 35–45° shows likely bcc tungsten (110) in the form of nanograins; moreover, 10 L reflections of WSe_2 (L = 1, 2, …) may contribute to this peak as well, possibly with a turbstrating effect discussed above. The Raman spectrum shown in Fig. 1 (b) exhibits two significant regions in the spectrum of WSe_{2-x} coating. Peak at 245 cm^{-1} is very close to positions of E^1_{2g} and A_{1g} modes in 2H-WSe_2 [28] (note that the separation of these modes is almost negligible in WSe_2, about 8 cm^{-1}), suggesting that the 2H phase is predominant in the coating. A smaller peak is positioned close to 170 cm^{-1}, which can be identified as E_{1g} in 2H-WSe_2 [29]. Broad peaks at 807 cm^{-1} belong to WO_3, suggesting a small amount of oxidation in the coating, as already indicated by EDX measurement [30]. The Raman spectrum of MoS_2 shows peaks at 169 cm^{-1}, 371 cm^{-1}, and 405 cm^{-1}, fitting well with the typical Raman spectrum of 2H-MoS_2 [31]. Small peaks in the region of 750–930 cm^{-1} indicate the presence of oxide phases.

The X-ray photoelectron spectroscopy (XPS) was conducted on each coating to assess the surface chemistry state further. As illustrated in Fig. 2(a), the W 4f spectrum in WSe_{2-x} coatings contains W^{4+}, associated with WSe_2, W^{6+}, attributed to tungsten oxides, and W^0 corresponding with metallic state tungsten. The dual peaks at 32.2 eV and 34.1 eV correspond to the $4f_{5/2}$ and $4f_{7/2}$ levels of WSe_2, respectively [32]. Due to oxidation, sharp peaks are observed at 35.6 eV and 37.7 eV, which are linked to tungsten oxides (WO_x) [33,34]. Additionally, a small peak at 41.8 eV corresponds to W 5p, also associated with WO_x [35]. The peaks representing metallic tungsten can also be indexed at 31.4 eV and 33.4

Table 1
Deposition parameters for coatings.

Sample Name	Power (W)	Base Vacuum (Pa)	Working Pressure (Pa)	Deposition Time (s)	Thickness (nm)
MoS_2	150	5×10^{-3}	0.67	5400	1320
WSe_{2-x}	150	5×10^{-3}	0.67	7200	1030

Table 2
Chemical composition and mechanical properties of as-deposited coatings.

	Mo or W	S or Se	O	S/Mo or Se/W	Hardness (GPa)	Young's modulus (GPa)
MoS_2	30.1	57.3	12.6	1.91	0.5	25.4
WSe_{2-x}	47.7	44.1	8.2	0.92	3.5	87.7

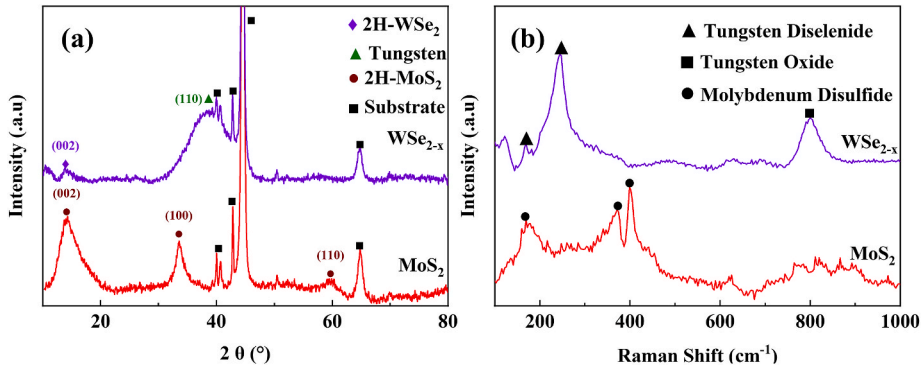

Fig. 1. Structural characteristics of as-deposition coatings: (a) XRD, (b) Raman spectroscopy.

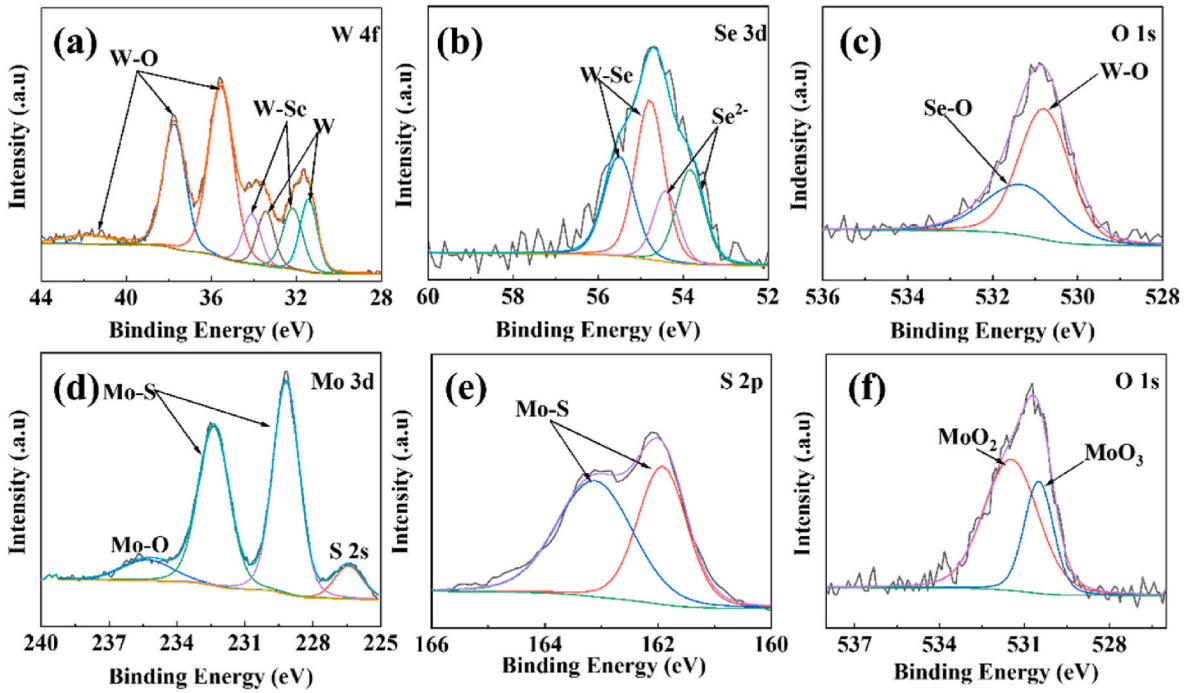

Fig. 2. X-ray photoelectron spectrum of WSe_{2-x}: (a) W 4f, (b) Se 3d, (c) O 1s; and of MoS_2: (d) Mo 3d, (e) S 2p, (f) O 1s.

eV [36]. Aside from the characteristic twin peaks at 54.7 eV and 55.5 eV for WSe_2 [37], another pair of peaks at 53.8 eV and 54.4 eV can is present. These extra peaks are often attributed to Se^{2-}, shifted likely due to the presence of oxygen combined with low selenium content in WSe_{2-x} coating [38]. O1s spectrum shows a broad peak at 531.3 eV, which fits O^{2-} in Se-O binding, while a W-O binding peak can also be recognized at 530.8 eV [39,40]. In the case of the as-deposited MoS_2 coating, Mo^{4+} is present in MoS_2, and Mo^{6+} is linked to molybdenum oxides. Two prominent peaks at 229.2 eV and 232.4 eV correspond to the Mo $3d_{5/2}$ and Mo $3d_{3/2}$ levels of MoS_2, respectively [41]. A small peak at 235.3 eV, corresponding to the Mo-O bond, indicates surface oxidation of the MoS_2 coating [42]. Two types of oxides can be detected in the MoS_2 coating from O1s spectrum (Fig. 2 (f)): MoO_2 with O^{2-} peak at 531.5 eV, and MoO_3 with O^{2-} peak positioned at 530.5 eV [43,44]. Note that metallic molybdenum was not observed, which corresponds well with a high stoichiometry of this coating.

Fig. 3 shows surface topography and friction force maps of coatings. WSe_{2-x} coating exhibits a compact cluster-like morphology with a low surface roughness Ra of around 4 nm. MoS_2 coating surface, in contrast, includes many holes (Fig. 3(c)), contributing to rougher morphology with a higher surface roughness (Ra~28.8 nm).

3.2. Macroscale tribological testing: load dependence

The frictional properties of the as-deposited coatings were evaluated using a UMT-2 tribometer under ambient conditions. The friction curves are shown in Fig. S3. As shown in Fig. 4, WSe_{2-x} coatings demonstrated a very low coefficient of friction in the ambient environment, decreasing with increasing normal load from 0.083 to 0.054. MoS_2 follows the same trend, but with much higher values in a range of 0.248–0.075. The average coefficient of friction of TMD solid lubricants is often fitted using Hertz contact [45]:

$$\mu = \tau_0 \pi \left(\frac{3R}{4E}\right)^{2/3} L^{-2/3} + \alpha, \qquad \text{Equation (2)}$$

Where μ is the coefficient of friction, τ_0 is the shear strength at the tribological interface, R is the radius of the ball, E is Young's modulus, L is the normal load, and α is the coefficient representing the coefficient of friction at zero loads (component related mostly to surface adhesion). As shown in Fig. 4 (b), the coefficient of friction of both coatings fits well Equation (1) with τ_0 of WSe_{2-x} and MoS_2 coatings calculated as 10.9 ± 0.2 and 36.8 ± 0.6 MPa, respectively. The value for MoS_2 corresponds well with the literature [46].

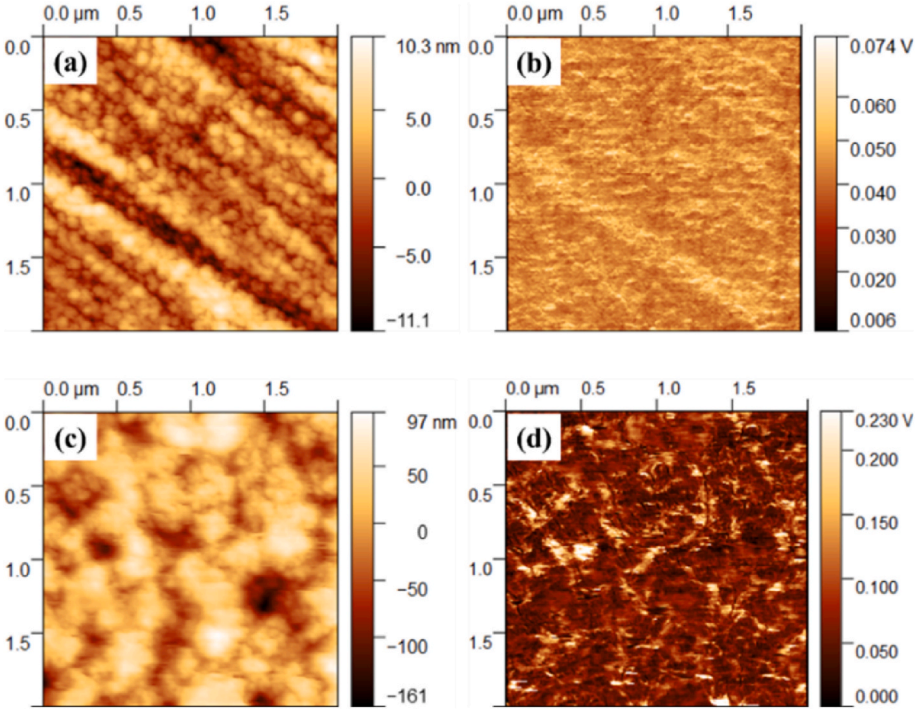

Fig. 3. Surface topographies of WSe_{2-x} (a) and MoS_2 (c) and corresponding friction force maps: WSe_{2-x} (b) and MoS_2 (d).

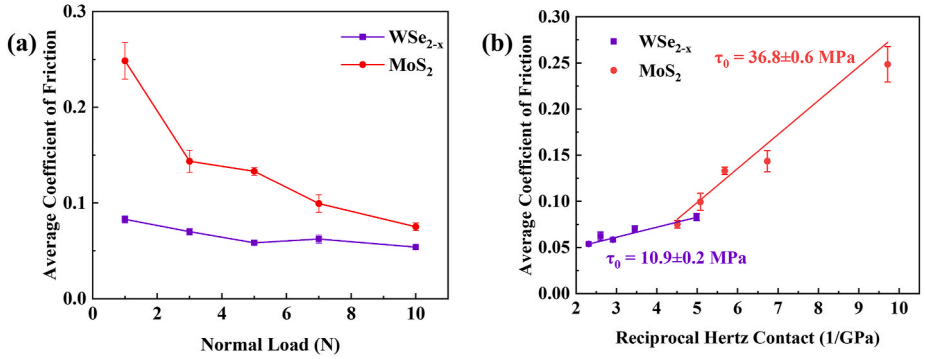

Fig. 4. (a) The average coefficient of friction of WSe_2 and MoS_2 coatings and (b) linear regression fit of steady-state coefficient of friction of WSe_2 and MoS_2.

3D topography of the wear tracks are presented in Fig. S4, with corresponding optical images provided in Fig. S5. Pronounced grooves were observed on all wear tracks of the WSe_{2-x} coatings, particularly at 7 N and 10 N. By contrast, the loose structure of the MoS_2 coating was compressed during testing, resulting in a flat and smooth worn surface.

The worn volumes and corresponding wear rates are shown in Fig. 5. WSe_{2-x} coating wear volume increases with the normal load up to 7 N; then it slightly decreases, a behavior observed in other TMD-based coatings as well [47]. MoS_2 coating showed a similar trend, an increase in wear volume up to a maximum at a normal load of 7 N. As a consequence, the wear rate of both coatings decreases with the applied load, but the wear rate of WSe_{2-x} is significantly lower in the entire load range. The wear on the counterparts is very low for both coatings, with wear rates below 1×10^{-6} mm^3/Nm as shown in Fig. 5 (d). The balls sliding against WSe_{2-x} exhibit higher wear rates than those sliding against MoS_2; nevertheless, the ball wear shows different trends for the two solid lubricant coatings. Unlike continuously decreasing MoS_2 ball wear with load, WSe_{2-x} ball wear shows more or less random evolution independent of normal load.

Fig. 6 shows Raman spectra taken from the wear track. MoS_2 underwent significant recrystallization during sliding. Distinct peaks at around 400 cm^{-1}, corresponding to the 2H-MoS_2 phase, are present in all post-test spectra. Moreover, the peaks (E_{2g} and A_{1g}) slightly shifted from an initial (unworn surface) position when acquired from the wear track, but the peak position remained almost independent of the applied load. However, it is worth noting that the peaks of the as-deposited surface are not well defined, and identification of their position is difficult. WSe_2 spectra from the wear tracks were very similar to that of the as-deposited coating, and the shift of E_{12g} and A_{1g} peaks shown in Fig. S6 is quite random, although always moving into higher peak positions. Higher values of E_1g peak indicate a different structure of the worn surface [44,45], but our Raman spectra are not conclusive to state that a WSe_2 tribolayer with a higher degree of crystallinity has been formed.

As expected, a friction-induced material transfer from the wearing coating to the counterparts (balls) occurred for both solid lubricants (Fig. S7 and Fig. S8). Raman spectra taken from the center of transferred materials adhering to ball scars are shown in Fig. 6. Both WSe_{2-x} and MoS_2 show significant Raman peaks for 2H-WSe_2 and 2H-MoS_2 for all loads. Note that there is almost no oxidation, as demonstrated by the absence of peaks at ~820 cm^{-1} for Mo-O_x and ~810 cm^{-1} for W-O_x [30, 48]. Moreover, there is no evidence of Raman peak in positions close to

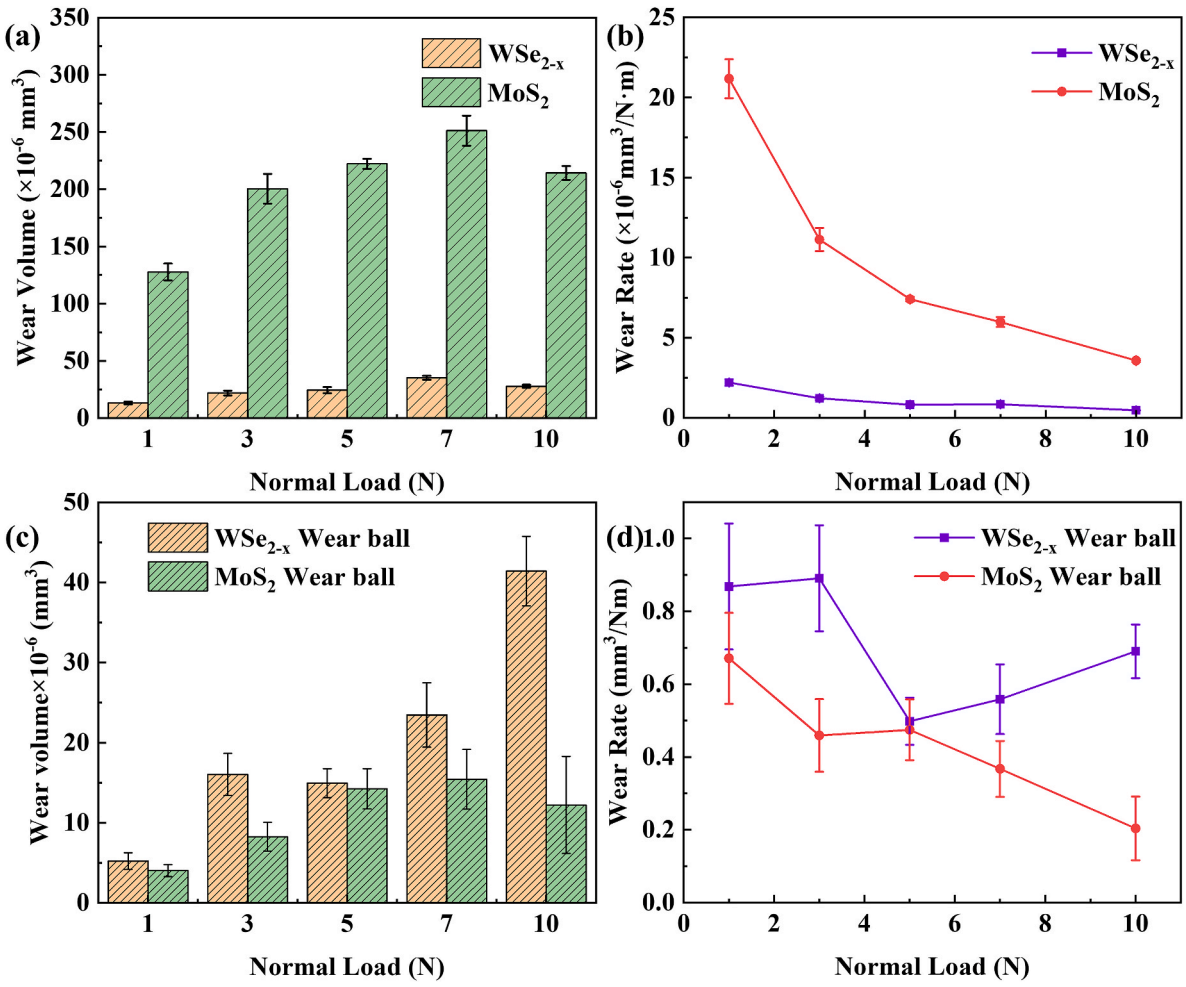

Fig. 5. (a) The worn volumes and (b) corresponding wear rate of WSe_{2-x} and MoS_2 coatings; (c) the worn volumes and (d) corresponding wear rate of WSe_{2-x} and MoS_2 wear balls.

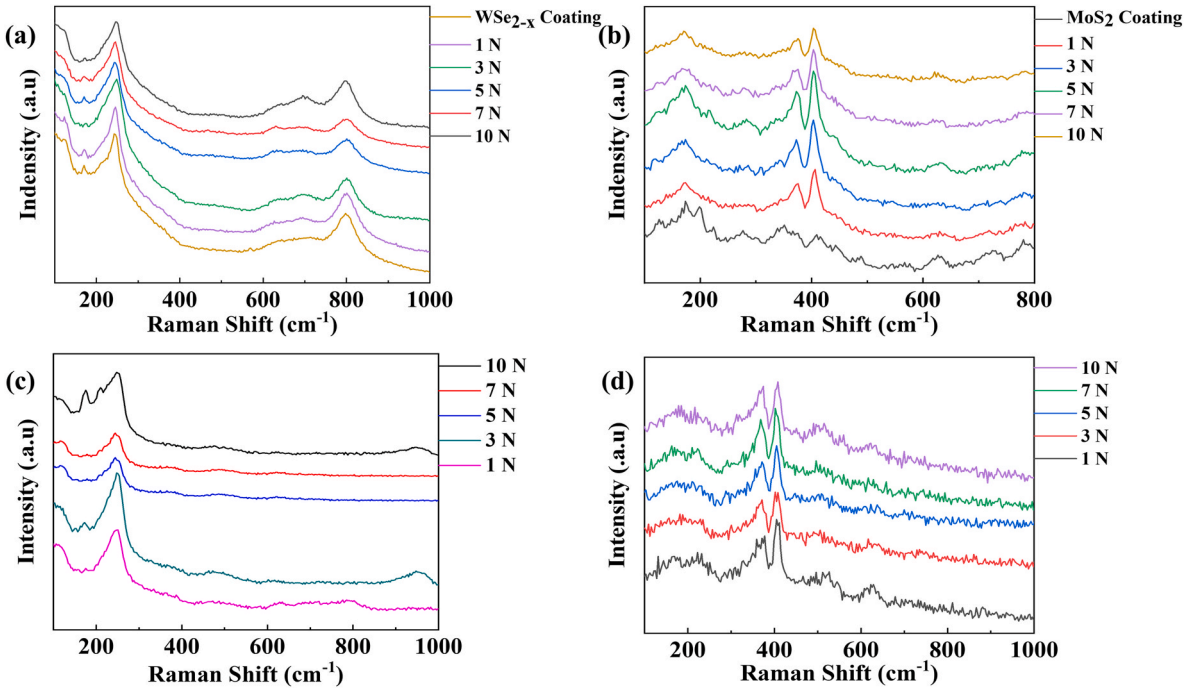

Fig. 6. Raman spectra on the wear tracks: (a) WSe_{2-x} coating, (b) MoS_2 coating; and on the ball scars: (c) WSe_{2-x}, (d) MoS_2.

iron oxides or more complex iron-based compounds (Table 3). These results indicate that the ball wear is likely caused during running in, and then the wear scar is covered (and protected) by material transferred from the solid lubricant coatings. The position of peaks shown in Fig. S9 is very similar to that of the wear track. Combining the morphology and Raman spectra, the WSe_{2-x} shows a lower amount of coating material transferred to the ball when compared to MoS_2, which can contribute to slightly higher ball wear during sliding with WSe_{2-x} coating. Nevertheless, we can conclude here that the ball wear is negligible in both cases, limited to the initial running-in stage, and does not significantly influence the tribological properties of the coatings.

Fig. 7 provides a more precise representation of the wear track surface structure evolution through the ratio of peak intensities. The tribo-active structure change is profound on MoS_2 coatings as the ratio of $I(A_{1g})/I(E_{2g})$ is much higher on transfer layers and wear tracks when compared to the as-deposited coating. Thus, it is clear evidence of the formation of a highly crystalline tribolayer. As the $I(A_{1g})/I(E_{2g})$ ratio does not change with increasing normal load, it is evident that the transformation of the wearing surface is completed already at the lowest load. The peak intensity ratio $I(E_{1g})/I(E^1_{2g} + A_{1g})$ is almost identical to as-deposited coating surface in the case of WSe_{2-x} coatings; it increases only in the case of the highest load.

3.3. Nanotribological testing: wear track analysis

Nanotribological test was deployed on both TMD-based coatings to evaluate the tribological mechanism of WSe_{2-x} coating. Nanotribological testing and surface topography were collected by SPM on 1 N and 10 N wear tracks. A 2 μm × 2 μm region was selected at the center of the wear track to avoid any macroscale defects. Fig. 8 shows topographies of wear tracks for 1 N and 10 N testing on the WSe_{2-x} sample. Roughness is slightly higher than for unworn coating: Ra~8.2 nm for 1 N wear track and Ra~5.4 nm for 10 N wear track. The friction map in Fig. 8 (b) is uniform and independent of topography under low contact stress. Meanwhile, the topography of the 10 N wear track showed several small (50–300 nm) particles adhered on the surface, which exhibited significantly lower friction than the rest of the wear track (Fig. 8 (d)). These particles are almost identical in size and friction to those observed by Rapuc et al. [53].

Compared with the WSe_{2-x} sample, sputtered MoS_2 shows uniform friction maps, and no particles were observed at any of the worn surfaces, see Fig. 9. At the highest load (10N), the surface was noticeably polished with Ra~4.8 nm.

Finally, a load-dependent friction testing was also carried out on the as-deposited coating surface and inside the selected wear tracks (region of 2 μm × 2 μm). The coefficient of friction was significantly lower inside all wear tracks, as shown in Fig. 10. Moreover, the coefficient of friction on the wear tracks produced at 10 N load is lower than that of wear tracks produced with 1N load. It is worth noting that MoS_2 coatings exhibit a much higher drop in friction when measured outside and inside the wear tracks, suggesting strong structural (crystalline tribolayer formation) and topographical (polishing) transformation of the worn surface.

Table 3
Raman peak positions of potential iron-based oxide tribochemical products.

Phases	Raman peak positions (cm^{-1})
Fe_2O_3	229, 294, 410 cm^{-1} [49]
Fe_3O_4	532, 667 cm^{-1} [49]
β-$FeMoO_4$	943 cm^{-1} [50]
$FeWO_4$	878 cm^{-1} [51,52]

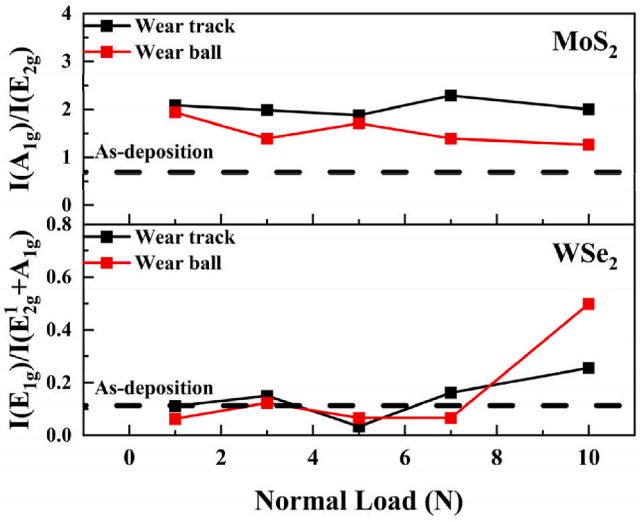

Fig. 7. The intensity ratios of the A_{1g} and E_{2g} peaks for MoS_2, and the E_{1g} and $(E^1_{2g} + A_{1g})$ peaks for WSe_2.

3.4. The effect of variable load during the sliding

As shown above, WSe_{2-x} coating shows a load dependence of the coefficient of friction typical of TMD materials, which decreases with normal load. However, there is still an open question about the mechanisms. In general, lower friction at higher loads is attributed to a better-developed (thicker, more aligned) TMD tribolayer. Consequently, if we produce the tribolayer at a high load, the friction should then stay the same when the tribological test continues at a lower load. To test this hypothesis, we performed a sliding test of WSe_{2-x} coating with periodic change of load from 1 to 10 N every 200 laps, see Fig. 11. If we excluding the first 200 laps at 1 N, where elevated friction is clearly attributed to running-in, the average CoF for 10 N started at 0.056 and slowly decreased to 0.051 for the last 200 laps. For 1N, the CoF decreased slightly from 0.068 to 0.063 as well. Note that the change in coefficient of friction is abrupt when the load is adjusted in both directions, strongly suggesting that it is not related to structural/morphological changes of the tribolayer.

3.5. The effect of humidity

Air humidity is a crucial factor influencing the lubrication properties of TMDs by increasing interlayer shear strength [45]. High humidity leads to a high coefficient of friction, as documented for MoS_2 [54] and WS_2 [55]; however, such an effect is much weaker for diselenides [10]. We performed sliding tests in vacuum (under 7×10^{-3} Pa) at 1 N and 10 N normal load (Fig. S10); the WSe_{2-x} coating showed similar frictional response both in absolute value and load dependence (in vacuum, the coefficient of friction was 0.085 and 0.058 for 1 and 10 N, respectively).

4. Discussion

4.1. Friction and wear mechanisms of WSe_{2-x} coating

We combine our experiments with literature to elucidate possible dominant tribological mechanisms. The nanofriction maps produced by AFM clearly show that the coefficient of friction in the wear track is much less uniform when compared to the as-deposited coating, indicating a combination of morphological and structural changes at the surface. The coefficient of friction in the wear tracks is lower in both TMDs; for WSe_{2-x}, the value dropped from 0.64 (free surface) to 0.47 (1N wear track) and to 0.25 (10N wear track). Although the sliding induced recrystallization and formation of well-aligned (with basal planes

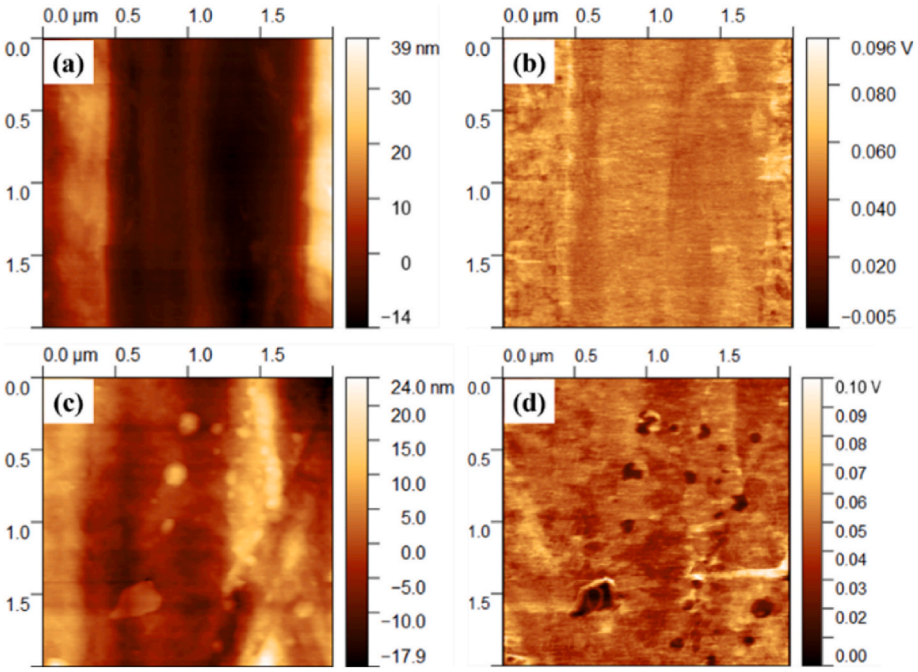

Fig. 8. Topographies and friction maps of wear tracks on WSe_{2-x} sample: (a) and (b) 1 N, (c) and (d) 10 N.

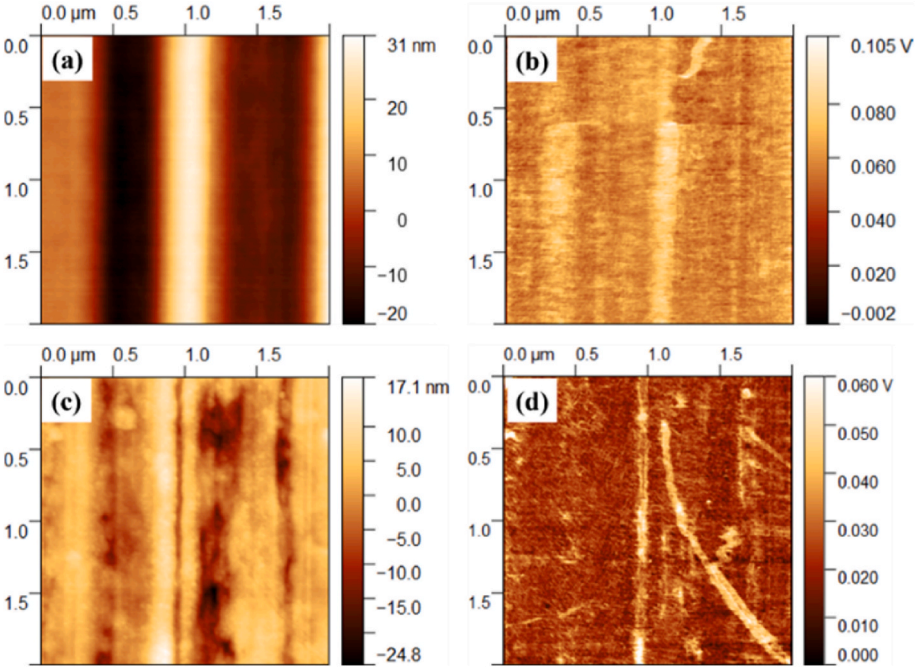

Fig. 9. Topographies and friction maps of wear tracks on MoS_2 sample: (a) and (b) 1 N, (c) and (d) 10 N.

parallel to the surface) crystalline tribolayers on the wear track is the most likely explanation, we have to assess first other possible key players, such as oxidation and the effect of roughness.

Sliding at room temperature with our sliding speed and load range significantly reduces the detrimental effect of direct surface oxidation. Indeed, the Raman analysis of the transferred material to the balls showed only crystalline TMD material and no oxides. High roughness increases nanofriction, but in our case, the coefficient of friction decreased significantly despite a rougher wear track surface. Thus, the oxidation effect is negligible, and the change in roughness cannot explain the observed frictional behavior. Consequently, the most likely explanation is the transformation of the wearing surface from a less ordered (polycrystalline) surface to a more ordered tribolayer. Typical tribolayers of TMD-based coatings are predominantly formed through tribochemical process (diffusion-driven), which produces almost pure 2D TMD sheets at the wearing surface. Such tribolayers formation is not hindered by nonstoichiometric composition [24,50]. Contamination or alloying element(s) in the coatings, such as O [48], C [47] or N [56]) (even with very high concentrations) are removed from the contact area. Therefore, the absence of oxides in transferred material to the ball wear scar indirectly indicates the formation of such a tribolayer. Direct analysis of the wear tracks by Raman spectroscopy clearly identified

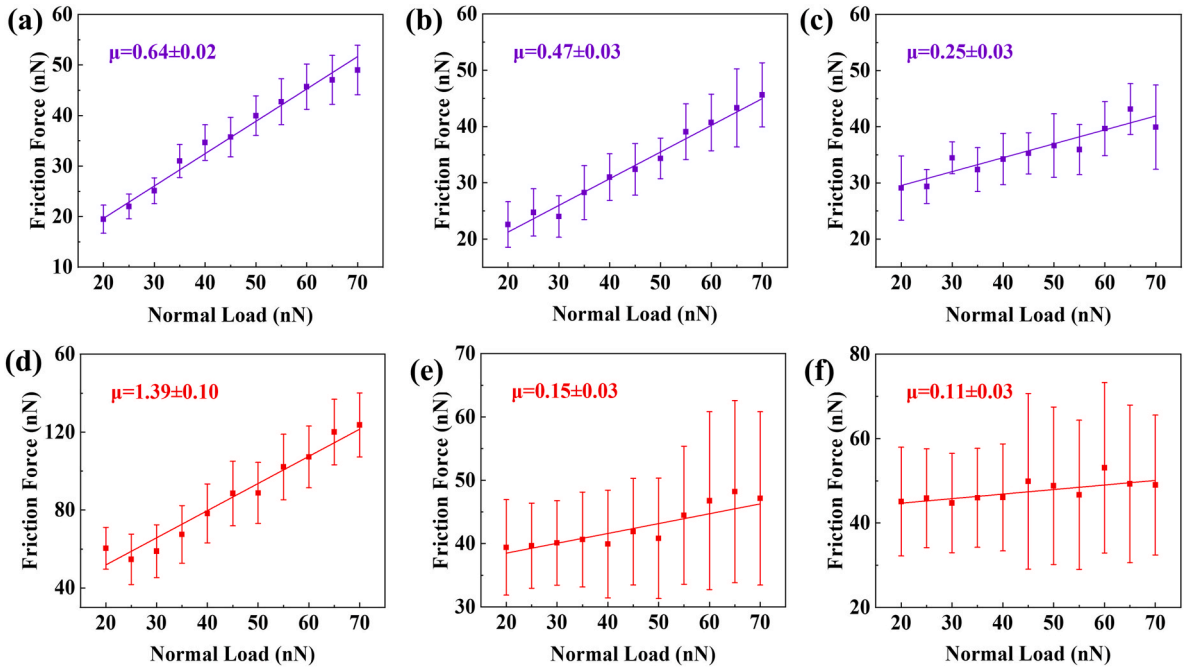

Fig. 10. Load dependence nanofriction result of WSe_{2-x}: (a) coating, (b) 1 N wear track, and (c) 10 N wear track; nanofriction result of MoS_2: (d) coating, (e) 1 N wear track, and (f) 10 N wear track.

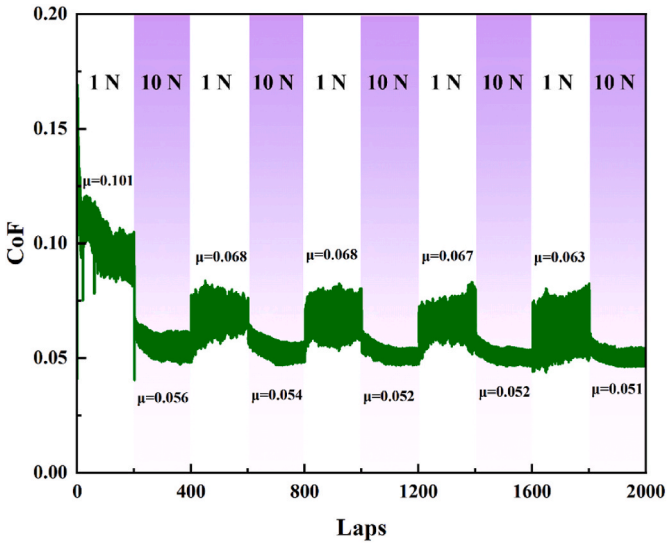

Fig. 11. Coefficient of friction of WSe_{2-x} coating with periodic change of normal load between 1 N and 10 N.

higher crystallinity of MoS_2; however, it was much less evident in the case of WSe_{2-x} due to the more pronounced initial (as-deposited) crystallinity of this coating. Nevertheless, it seems that the formation of WSe_2 tribolayer requires a higher energy input (provided by load) when compared to that of MoS_2. The drop in nanoscale coefficient of friction for MoS_2 is significant (about one order of magnitude) and the value is almost the same for 1 and 10 N load; for WSe_{2-x}, we observe a much smaller decrease in coefficient of friction in 1N wear track (0.6–0.47) with a further significant decrease in case of 10 N wear track (0.25). Moreover, the presence of low friction areas (Fig. 8 d) is a clear indication that the well-ordered tribolayer is formed in larger quantities only during the sliding at higher contact pressures.

Raman spectroscopy provides similar evidence that WSe_2 tribolayer requires higher energy input than that of MoS_2. E_{1g} peak position for WSe_2 shifts significantly at the highest load (10 N), while the peak for MoS_2 remains relatively unchanged (Fig. 6). Additionally, the intensity ratio of $I(A_{1g})$ to $I(E_{2g})$ in Raman spectra (Fig. 7) is independent of load, suggesting that the tribolayer fully forms even at the lowest load. The same ratio for WSe_2 changes significantly at the highest load, corroborating nanoscale friction testing.

We can conclude here that there is strong indirect evidence of tribolayer formation in the wear track of WSe_{2-x} coating, although individual techniques, such as Raman spectroscopy, provide only limited information due to the polycrystalline nature of the film. It is likely that high deficiency in selenium, resulting in high hardness, limits the formation of a low-friction tribolayer at lower loads. Thus, the drop in coefficient of friction with increasing load from 0.083 at 1 N to 0.054 at 10 N (Fig. 4 and Fig. S3) closely follows behavior observed in other TMD-based coatings [57–59], where enhanced tribolayer formation leads to reduced macroscale friction. Moreover, there is strong indirect evidence of the tribolayer formation – transfer of the coating material on the ball wear scar, clearly evident for MoS_2 and, to a lesser extent, for WSe_{2-x} coating as well (Fig. S7). Such a transferred tribolayer is typical of TMD-based coatings [60].

Cyclic change of load resulted in reproducible oscillation of the coefficient of friction. A rapid drop (when the load increases) or rise (when the load is lowered) in friction suggests that a structural change of the wear track surface (in other words, a change of the tribolayer) is an unlikely factor explaining the sudden jump in friction. Thus, we are left with two major factors: (i) the direct effect of load on sliding, where higher compression reduces the intrinsic friction of WSe_2 monolayers and/or affects the interaction with water molecules, and (ii) the indirect effect due to increased energy input resulting in higher contact temperature. For the first hypothesis, there is no evidence in the literature that higher load causes a drop in friction for the genuine (with no substrate effects) sliding of 2D TMD materials. Indeed, our previous study on MoS2 friction using density functional theory suggests an increasing barrier to sliding motion (and hence friction) when the contact pressure was increased [55]; moreover, we did not observe any decrease in the coefficient of friction during sliding of homo and heterostructures with MoS_2 studied both experimentally (sliding of small 2D flakes) and theoretically (molecular dynamics) [47]. For the second hypothesis, we

performed additional experiments to demonstrate whether higher contact temperature may reduce the friction. Fig. S11 shows the temperature dependence of the coefficient of friction. At a temperature range of 100–300 °C, the CoF reduced to a very low value of 0.020–0.025 when a load of 5N was used. Note that in this case, a silicon nitride ball was used as a counterpart to avoid rapid 100Cr6 oxidation and softening. High temperature can contribute to low friction by the reduction of sliding resistance (e.g., adhesion caused by van der Waals forces), or by drying of the atmosphere (humidity close to the heated coating surface is negligible). However, our WSe_{2-x} coating's frictional response to humidity is very low, as shown in section 3.5. Therefore, we can conclude here that, once the surface is polished and tribolayer is formed, the load-dependence of the coefficient of friction is primarily caused by increased contact temperature when the load is higher.

4.2. Tribological performance of WSe_{2-x} coating in the context of solid lubricants

Despite a high deficiency in selenium, WSe_{2-x} coating shows excellent sliding properties with a very low coefficient of friction, decreasing with higher applied loads. WSe_{2-x} coating friction is not sensitive to humid air (see Fig. S10) and outperforms most of the other transition metal dichalcogenide-based coatings. To support such a statement, we compare our results with those reported in the literature for pure and doped MoS_2 coatings [24,56,61–69], WS_2-based coatings [70–75], and $MoSe_2$ based coatings [76,77], as illustrated in Fig. 12. The values were obtained under similar conditions (sliding against a steel ball in humid air). A very low value of shear strength calculated from Equation (1) (Fig. 5), which is almost four times lower than that of MoS_2, further indicates the potential of tungsten diselenide as a solid lubricant.

Similarly, the wear rates of WSe_{2-x} coating in this study, 0.46×10^{-6} to 2.20×10^{-6} mm^3/Nm, are much lower than our reference MoS_2 coating or similar coatings reported elsewhere [70,78–80]. It is worth noting that, thanks to a tribolayer formation, the coefficient of friction for various coatings (e.g., MoS_2) is relatively comparable. However, the wear rate is much more dependent on coating hardness, density, and structure, so the direct comparison of the wear rates is only indicative.

5. Conclusion

This study investigated tribological properties of solid lubricant WSe_{2-x} coating deposited by magnetron sputtering and compared it to well established MoS_2 deposited under identical conditions. The coating was tungsten-rich with a Se/W ratio of 0.92; structural analysis showed a mixture of WSe_2 and metallic tungsten phases, which contributed to high hardness and Young's modulus. Both WSe_{2-x} and MoS_2 showed similar non-Amontonian tribological behavior – the coefficient of friction decreased with increasing load thanks to the formation of a well-oriented tribolayer identified by surface analyses and nanotribological tests. However, WSe_{2-x} required higher energy input to form such tribolayer, likely due to a low Se/W ratio. The wear of the film was significantly lower than that of MoS_2, demonstrating the promising tribological potential of tungsten diselenide. Furthermore, the friction performance of the WSe_{2-x} coating was similar under ambient and vacuum conditions, indicating a reduced sensitivity to oxidation and humidity.

CRediT authorship contribution statement

Yue Wang: Writing – original draft, Methodology, Investigation, Data curation. **Himanshu Rai:** Investigation. **Tomas Polcar:** Writing – review & editing, Supervision, Project administration, Funding acquisition, Conceptualization.

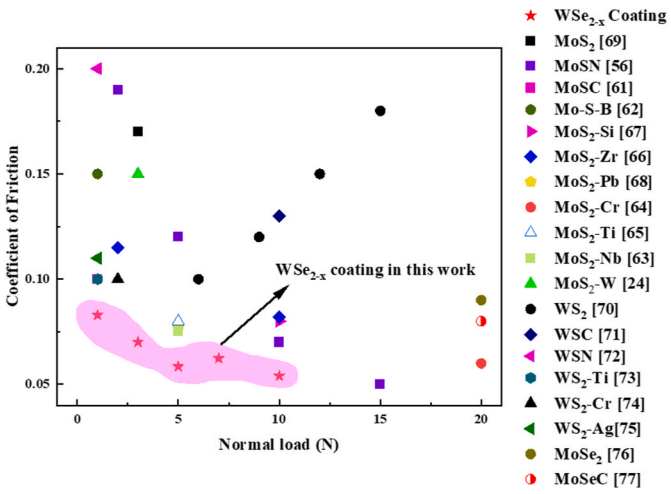

Fig. 12. The comparison of WSe_{2-x} coating and other TMDs based solid lubricating coatings.

Declaration of competing interest

The authors declare the following financial interests/personal relationships which may be considered as potential competing interests: Tomas Polcar reports financial support was provided by GACR through grant 23-07785S and co-funded by the European Union under the project Robotics and advanced industrial production (CZ.02.01.01/00/22_008/0004590). If there are other authors, they declare that they have no known competing financial interests or personal relationships that could have appeared to influence the work reported in this paper.

Acknowledgments

This work was supported by GACR through grant 23-07785S and co-funded by the European Union under the project Robotics and advanced industrial production (CZ.02.01.01/00/22_008/0004590).

Appendix A. Supplementary data

Supplementary data to this article can be found online at https://doi.org/10.1016/j.wear.2025.206305.

Data availability

Data will be made available on request.

References

[1] T.W. Scharf, S.V. Prasad, Solid lubricants: a review, J. Mater. Sci. 48 (2013) 511–531, https://doi.org/10.1007/s10853-012-7038-2.
[2] M.R. Vazirisereshk, A. Martini, D.A. Strubbe, M.Z. Baykara, Solid lubrication with MoS2: a review, Lubricants 7 (2019), https://doi.org/10.3390/LUBRICANTS7070057.
[3] K.P. Furlan, J.D.B. de Mello, A.N. Klein, Self-lubricating composites containing MoS_2: a review, Tribol. Int. 120 (2018) 280–298, https://doi.org/10.1016/j.triboint.2017.12.033.
[4] S.H. Mukhtar, A. Gulzar, S. Saleem, M.F. Wani, R. Sehgal, A.A. Yakovenko, I. G. Goryacheva, M.D. Sharma, Advances in development of solid lubricating MoS_2 coatings for space applications: a review of modeling and experimental approaches, Tribol. Int. 192 (2024) 109194, https://doi.org/10.1016/J.TRIBOINT.2023.109194.
[5] T. Arif, S. Yadav, G. Colas, C.V. Singh, T. Filleter, Understanding the independent and interdependent role of water and oxidation on the tribology of ultrathin molybdenum disulfide (MoS_2), Adv. Mater. Interfac. 6 (2019), https://doi.org/10.1002/admi.201901246.
[6] Z. Yang, S. Bhowmick, F.G. Sen, A.T. Alpas, Microscopic and atomistic mechanisms of sliding friction of MoS_2: effects of undissociated and dissociated H_2O, Appl. Surf. Sci. 563 (2021), https://doi.org/10.1016/j.apsusc.2021.150270.

[7] J.R. Lince, S.H. Loewenthal, C.S. Clark, Tribological and chemical effects of long term humid air exposure on sputter-deposited nanocomposite MoS_2 coatings, Wear (2019) 432–433, https://doi.org/10.1016/j.wear.2019.202935.

[8] S. Park, A.T. Garcia-Esparza, H. Abroshan, B. Abraham, J. Vinson, A. Gallo, D. Nordlund, J. Park, T.R. Kim, L. Vallez, R. Alonso-Mori, D. Sokaras, X. Zheng, Operando study of thermal oxidation of monolayer MoS_2, Adv. Sci. 8 (2021), https://doi.org/10.1002/advs.202002768.

[9] H. Cao, J. Momand, A. Syari'ati, F. Wen, P. Rudolf, P. Xiao, J.T.M. De Hosson, Y. Pei, Temperature-adaptive ultralubricity of a WS_2/a-C nanocomposite coating: performance from room temperature up to 500 °c, ACS Appl. Mater. Interfaces 13 (2021) 28843–28854, https://doi.org/10.1021/acsami.1c06061.

[10] T. Kubart, T. Polcar, L. Kopecký, R. Novák, D. Nováková, Temperature dependence of tribological properties of MoS_2 and $MoSe_2$ coatings, Surf. Coat. Technol. 193 (2005) 230–233, https://doi.org/10.1016/j.surfcoat.2004.08.146.

[11] A. Rapuc, H. Wang, T. Polcar, Nanotribology of transition metal dichalcogenide flakes deposited by chemical vapour deposition: the influence of chemical composition and sliding speed on nanoscale friction of monolayers, Appl. Surf. Sci. 556 (2021), https://doi.org/10.1016/j.apsusc.2021.149762.

[12] S. Dominguez-Meister, A. Justo, J.C. Sanchez-Lopez, Synthesis and tribological properties of WSe_x films prepared by magnetron sputtering, Mater. Chem. Phys. 142 (2013) 186–194, https://doi.org/10.1016/j.matchemphys.2013.07.004.

[13] M. Evaristo, T. Polcar, A. Cavaleiro, Can W-Se-C coatings be competitive to W-S-C ones? Plasma Process. Polym. (2009) https://doi.org/10.1002/ppap.200930414.

[14] A. Pauschitz, E. Badisch, M. Roy, D.V. Shtansky, On the scratch behaviour of self-lubricating WSe_2 films, Wear 267 (2009) 1909–1914, https://doi.org/10.1016/j.wear.2009.03.037.

[15] D.V. Shtansky, A.N. Sheveyko, D.I. Sorokin, L.C. Lev, B.N. Mavrin, P. V. Kiryukhantsev-Korneev, Structure and properties of multi-component and multilayer TiCrBN/WSe_x coatings deposited by sputtering of TiCrB and WSe2 targets, Surf. Coat. Technol. 202 (2008) 5953–5961, https://doi.org/10.1016/j.surfcoat.2008.06.177.

[16] C. Tan, X. Zong, W. Zhou, H. Cao, J. Wang, C. Wang, J. Peng, Y. Li, H. Li, J. Wang, S. Chen, Insights into the microstructure characteristics, mechanical properties and tribological behaviour of gas-phase chromized coating on GCr15 bearing steel, Surf. Coat. Technol. 443 (2022), https://doi.org/10.1016/j.surfcoat.2022.128605.

[17] H. Rai, D. Thakur, D. Kumar, A. Pitkar, Z. Ye, V. Balakrishnan, N.N. Gosvami, Spatial variation in nanoscale wear behavior of chemical vapor deposited monolayer WS_2, Appl. Surf. Sci. 605 (2022) 154783, https://doi.org/10.1016/J.APSUSC.2022.154783.

[18] H. Rai, D. Thakur, A. Gadal, Z. Ye, V. Balakrishnan, N.N. Gosvami, Nanoscale friction and wear behavior of a CVD-grown aged WS_2 monolayer: the role of wrinkles and surface chemistry, Nanoscale (2023) 10079–10088, https://doi.org/10.1039/d3nr01261a.

[19] J.E. Sader, I. Larson, P. Mulvaney, L.R. White, Method for the calibration of atomic force microscope cantilevers, Rev. Sci. Instrum. 66 (1995) 3789–3798, https://doi.org/10.1063/1.1145439.

[20] C.P. Green, H. Lioe, J.P. Cleveland, R. Proksch, P. Mulvaney, J.E. Sader, Normal and torsional spring constants of atomic force microscope cantilevers, Rev. Sci. Instrum. 75 (2004) 1988–1996, https://doi.org/10.1063/1.1753100.

[21] H. Rai, D. Thakur, A. Gadal, Z. Ye, V. Balakrishnan, N.N. Gosvami, Transforming friction: unveiling sliding-induced phase transitions in CVD-grown WS_2 monolayers under single-asperity sliding nanocontacts, Nanoscale 16 (2024) 7102–7109, https://doi.org/10.1039/D3NR06556A.

[22] N.N. Gosvami, J. Ma, R.W. Carpick, An in situ method for simultaneous friction measurements and imaging of interfacial tribochemical film growth in lubricated contacts, Tribol. Lett. (2018), https://doi.org/10.1007/s11249-018-1112-0.

[23] S. Domínguez-Meister, T.C. Rojas, M. Brizuela, J.C. Sánchez-López, Solid lubricant behavior of MoS_2 and WSe_2-based nanocomposite coatings, Sci. Technol. Adv. Mater. 18 (2017) 122–133, https://doi.org/10.1080/14686996.2016.1275784.

[24] Y. Wang, J. He, X. Song, W. Zhou, S. Chen, Y. Chen, Y. Cai, J. Wang, H. Li, Microstructure and tribological properties of sputtered MoS_x-W composite films supported by porous alumina aperture array, Surf. Coat. Technol. 450 (2022), https://doi.org/10.1016/j.surfcoat.2022.128958.

[25] K. Zhu, L. Luo, T. Peng, Preparation, characterization, and catalytic performance of MoS_2 photocatalyst, J. Wuhan Univ. Technol.-Materials Sci. Ed. 34 (2019) 883–887, https://doi.org/10.1007/s11595-019-2132-9.

[26] J. Moser, F. Lrvy, Random stacking in MoS_{2-x} sputtered thin films, Thin Solid Films 240 (1994) 56–59, https://doi.org/10.1016/0040-6090(94)90693-9.

[27] D. Singh, A. Singh, S.K. Ojha, A.K. Ojha, Facile synthesis of layered 2H-WSe_2 nanosheets for asymmetric supercapacitor device application, Synth. Met. 293 (2023), https://doi.org/10.1016/j.synthmet.2022.117263.

[28] H. Li, G. Lu, Y. Wang, Z. Yin, C. Cong, Q. He, L. Wang, F. Ding, T. Yu, H. Zhang, Mechanical exfoliation and characterization of single- and few-layer nanosheets of WSe_2, TaS_2, and $TaSe_2$, Small 9 (2013) 1974–1981, https://doi.org/10.1002/smll.201202919.

[29] C.S. Rout, D.J. Late, eds., Advanced Analytical Techniques for Characterization of 2D Materials, AIP Publishing LLC, 10AD. https://doi.org/10.1063/9780735425422.

[30] W. Song, R. Zhang, X. Bai, Q. Jia, H. Ji, Exposed crystal facets of WO_3 nanosheets by phase control on NO_2-sensing performance, J. Mater. Sci. Mater. Electron. 31 (2020) 610–620, https://doi.org/10.1007/s10854-019-02565-6.

[31] T. Vitu, T. Huminiuc, G. Doll, E. Bousser, A. Matthews, T. Polcar, Tribological properties of Mo-S-C coating deposited by pulsed d.c. magnetron sputtering, Wear (2021) 480–481, https://doi.org/10.1016/j.wear.2021.203939.

[32] M. Yamamoto, S. Dutta, S. Aikawa, S. Nakaharai, K. Wakabayashi, M.S. Fuhrer, K. Ueno, K. Tsukagoshi, Self-limiting layer-by-layer oxidation of atomically thin WSe2, Nano Lett. 15 (2015) 2067–2073, https://doi.org/10.1021/nl5049753.

[33] M. Occhiuzzi, D. Cordischi, D. Gazzoli, M. Valigi, P.C. Heydorn, WO_x/ZrO_2 catalysts part 4. Redox properties as investigated by redox cycles, XPS and EPR, Appl. Catal. Gen. 269 (2004) 169–177, https://doi.org/10.1016/j.apcata.2004.04.013.

[34] A.K. Mohamedkhair, Q.A. Drmosh, M. Qamar, Z.H. Yamani, Tuning structural properties of WO_3 thin films for photoelectrocatalytic water oxidation, Catalysts 11 (2021) 1–16, https://doi.org/10.3390/catal11030381.

[35] K. Mullapudi, K.E.K. Holden, J.L. Peterson, C.L. Dezelah, D.F. Moser, R.K. Kanjolia, D.J. Tweet, J.F. Conley, Plasma-enhanced atomic layer deposition of WO_3-SiO_2 films using a heteronuclear precursor, J. Vac. Sci. Technol. A 41 (2023), https://doi.org/10.1116/6.0002214.

[36] NIST X-ray photoelectron spectroscopy database, (n.d.). https://doi.org/10.18434/T4T88K.

[37] J. Kim, Y.R. Lim, Y. Yoon, W. Song, B.K. Park, J. Lim, T.M. Chung, C.G. Kim, A facile synthetic route to tungsten diselenide using a new precursor containing a long alkyl chain cation for multifunctional electronic and optoelectronic applications, RSC Adv. 9 (2019) 6169–6176, https://doi.org/10.1039/c9ra00041k.

[38] L. Sun, H. Xu, Z. Cheng, D. Zheng, Q. Zhou, S. Yang, J. Lin, A heterostructured WS_2/WSe_2 catalyst by heterojunction engineering towards boosting hydrogen evolution reaction, Chem. Eng. J. 443 (2022), https://doi.org/10.1016/j.cej.2022.136348.

[39] A. Sharma, N. Sharotri, P. Kandwal, R.K. Sharma, D. Sud, R. Rai, A. Hnydiuk-Stefan, Exploring the twin potential of nanostructured TiO_2:SeO_2 as a promising visible light photocatalyst and selective fluorosensing platform, Sci. Rep. 14 (2024), https://doi.org/10.1038/s41598-024-64167-5.

[40] A. Khan, S.N. Sapakal, A. Kadam, Tailoring tungsten trioxide (WO_3): ph-dependent synthesis, structural insights, and exceptional electrochromic performance, Sustainability 5 (2025) 100065, https://doi.org/10.1016/j.nxsust.2024.100065.

[41] R. Amin, M.A. Hossain, Y. Zakaria, Interfacial kinetics and ionic diffusivity of the electrodeposited MoS_2 film, ACS Appl. Mater. Interfaces 10 (2018) 13509–13518, https://doi.org/10.1021/acsami.8b01104.

[42] D. Barrera, Q. Wang, Y.J. Lee, L. Cheng, M.J. Kim, J. Kim, J.W.P. Hsu, Solution synthesis of few-layer 2H MX_2 (M = Mo, W; X = S, Se), J. Mater. Chem. C Mater. 5 (2017) 2859–2864, https://doi.org/10.1039/c6tc05097b.

[43] G.K. Sharma, J. Elkins, A.B. Puthirath, J. Murukeshan, A. Biswas, T.S. Pieshkov, A. Pramanik, R. Vajtai, D. Kaur, P.M. Ajayan, Binder-Free MoO_2-MoO_3 nanoarrays as high-performance anodes for Li-Ion batteries, Small 21 (2025), https://doi.org/10.1002/smll.202500361.

[44] H. Zhang, F. Li, H. Sheng, Y. Ma, J. Yuan, M. Shao, X. Zhu, H. Bi, Q. Su, Y. Zhang, W. Lan, Phase-engineered MoO_3/MoO_2 heterostructures for enhanced Zn2+/H+ pseudocapacitive storage in aqueous zinc-ion batteries, J. Colloid Interface Sci. 700 (2025), https://doi.org/10.1016/j.jcis.2025.138377.

[45] T.W. Scharf, P.G. Kotula, S.V. Prasad, Friction and wear mechanisms in MoS_2/Sb_2O_3/Au nanocomposite coatings, Acta Mater. 58 (2010) 4100–4109, https://doi.org/10.1016/j.actamat.2010.03.040.

[46] I.L. Singer, R.N. Bolster, J. Wegand, S. Fayeulle, B.C. Stupp, Hertzian stress contribution to low friction behavior of thin MoS_2 coatings, Appl. Phys. Lett. 57 (1990) 995–997, https://doi.org/10.1063/1.104276.

[47] K. Simonovic, T. Vitu, A. Cammarata, A. Cavaleiro, T. Polcar, Tribological behaviour of W-S-C coated ceramics in a vacuum environment, Tribol. Int. 167 (2022), https://doi.org/10.1016/j.triboint.2021.107375.

[48] A. Bondarev, I. Ponomarev, R. Muydinov, T. Polcar, Friend or foe? Revising the role of oxygen in the tribological performance of solid lubricant MoS_2, ACS Appl. Mater. Interfaces 14 (2022) 55051–55061, https://doi.org/10.1021/acsami.2c15706.

[49] P. Kumar, H. No-Lee, R. Kumar, Synthesis of phase pure iron oxide polymorphs thin films and their enhanced magnetic properties, J. Mater. Sci. Mater. Electron. 25 (2014) 4553–4561, https://doi.org/10.1007/s10854-014-2203-9.

[50] C. Zeng, J. Pu, H. Wang, S. Zheng, L. Wang, Q. Xue, Study on atmospheric tribology performance of MoS_2–W films with self-adaption to temperature, Ceram. Int. 45 (2019) 15834–15842, https://doi.org/10.1016/j.ceramint.2019.05.086.

[51] R. Schuler, F. Bianchini, T. Norby, H. Fjellvåg, Near-broken-gap alignment between $FeWO_4$ and Fe_2WO_6 for ohmic direct p-n junction thermoelectrics, ACS Appl. Mater. Interfaces 13 (2021) 7416–7422, https://doi.org/10.1021/acsami.0c19341.

[52] J. Qian, Z. Peng, D. Wu, X. Fu, $FeWO_4$/FeS core/shell nanorods fabricated by thermal evaporation, Mater. Lett. 122 (2014) 86–89, https://doi.org/10.1016/j.matlet.2014.02.001.

[53] A. Rapuc, K. Simonovic, T. Huminiuc, A. Cavaleiro, T. Polcar, Nanotribological investigation of sliding properties of transition metal dichalcogenide thin film coatings, ACS Appl. Mater. Interfaces 12 (2020) 54191–54202, https://doi.org/10.1021/acsami.0c16789.

[54] B. Vierneusel, T. Schneider, S. Tremmel, S. Wartzack, T. Gradt, Humidity resistant MoS_2 coatings deposited by unbalanced magnetron sputtering, Surf. Coat. Technol. 235 (2013) 97–107, https://doi.org/10.1016/j.surfcoat.2013.07.019.

[55] H. Cao, F. Wen, J.T.M. De Hosson, Y.T. Pei, Instant WS_2 platelets reorientation of self-adaptive WS_2/a-C tribocoating, Mater. Lett. 229 (2018) 64–67, https://doi.org/10.1016/j.matlet.2018.06.111.

[56] T. Hudec, M. Mikula, L. Satrapinskyy, T. Roch, M. Truchlý, P. Švec, T. Huminiuc, T. Polcar, Structure, mechanical and tribological properties of Mo-S-N solid lubricant coatings, Appl. Surf. Sci. 486 (2019) 1–14, https://doi.org/10.1016/j.apsusc.2019.03.294.

[57] K. Hebbar Kannur, T. Huminiuc, T. Bin Yaqub, T. Polcar, C. Pupier, C. Héau, A. Cavaleiro, An insight on the MoS_2 tribo-film formation to determine the friction performance of Mo-S-N sputtered coatings, Surf. Coat. Technol. 408 (2021), https://doi.org/10.1016/j.surfcoat.2020.126791.
[58] K. Dreva, A. Morina, L. Yang, A. Neville, The effect of temperature on water desorption and oxide formation in MoS_2 coatings and its impact on tribological properties, Surf. Coat. Technol. 433 (2022), https://doi.org/10.1016/j.surfcoat.2021.128077.
[59] A.V. Ayyagari, K.C. Mutyala, A.V. Sumant, Towards developing robust solid lubricant operable in multifarious environments, Sci. Rep. 10 (2020), https://doi.org/10.1038/s41598-020-72666-4.
[60] S. Krauß, A. Seynstahl, S. Tremmel, B. Meyer, E. Bitzek, M. Göken, T. Yokosawa, B. A. Zubiri, E. Spiecker, B. Merle, Structural reorientation and compaction of porous MoS_2 coatings during wear testing, Wear (2022) 500–501, https://doi.org/10.1016/j.wear.2022.204339.
[61] W. Dai, X. Li, L. Wu, Q. Wang, Structure and properties of molybdenum-disulfide/amorphous carbon composited coatings deposited by co-sputtering method, Diam. Relat. Mater. 101 (2020), https://doi.org/10.1016/j.diamond.2019.107643.
[62] W.D. Sun, X.L. Gu, L.N. Yang, J. Wang, K.F. Miao, C.Y. Dong, M. Wen, K. Zhang, Effect of boron content on the structure, mechanical and tribological properties of sputtered Mo–S–B films, Surf. Coat. Technol. 399 (2020), https://doi.org/10.1016/j.surfcoat.2020.126140.
[63] I. Efeoglu, Ö. Baran, F. Yetim, S. Altintaş, Tribological characteristics of MoS_2-Nb solid lubricant film in different tribo-test conditions, Surf. Coat. Technol. 203 (2008) 766–770, https://doi.org/10.1016/j.surfcoat.2008.08.048.
[64] X.Z. Ding, X.T. Zeng, X.Y. He, Z. Chen, Tribological properties of Cr- and Ti-doped MoS_2 composite coatings under different humidity atmosphere, Surf. Coat. Technol. 205 (2010) 224–231, https://doi.org/10.1016/j.surfcoat.2010.06.041.
[65] H. Li, G. Zhang, L. Wang, The role of tribo-pairs in modifying the tribological behavior of the MoS_2/Ti composite coating, J. Phys. D Appl. Phys. 49 (2016), https://doi.org/10.1088/0022-3727/49/9/095501.
[66] N.M. Renevier, V.C. Fox, D.G. Teer, J. Hampshire, Coating characteristics and tribological properties of sputter-deposited MoS_2-metal composite coatings deposited by closed field unbalanced magnetron sputter ion plating, Surf. Coat. Technol. 127 (2000), https://doi.org/10.1016/S0257-8972(00)00538-7.
[67] Y. Xu, M. Xie, Y. Li, G. Zhang, X. Xu, X. Fan, Q. Sun, H. Li, M. Zhu, The effect of Si content on the structure and tribological performance of MoS_2/Si coatings, Surf. Coat. Technol. 403 (2020), https://doi.org/10.1016/j.surfcoat.2020.126362.
[68] H. Li, G. Zhang, L. Wang, Low humidity-sensitivity of MoS_2/Pb nanocomposite coatings, Wear 350–351 (2016) 1–9, https://doi.org/10.1016/j.wear.2015.12.008.
[69] J. He, W. Zhou, S. Chen, A. Wu, Y. Zhou, Y. Chen, J. Wang, H. Li, Tribological properties of MoS_2 nano-flowers supported by porous alumina aperture array, Tribol. Int. 161 (2021), https://doi.org/10.1016/j.triboint.2021.107093.
[70] G. Wang, J. Song, G. Zhao, Q. Ding, T. Yin, H. Wang, Tribological performance prediction of WS_2 coating under different conditions by machine learning, Wear (2023) 532–533, https://doi.org/10.1016/j.wear.2023.205092.
[71] T. Vuchkov, V. Leviandhika, A. Cavaleiro, On the tribological performance of magnetron sputtered W-S-C coatings with conventional and graded composition, Surf. Coat. Technol. 449 (2022), https://doi.org/10.1016/j.surfcoat.2022.128929.
[72] P. Mutafov, M. Evaristo, A. Cavaleiro, T. Polcar, Structure, mechanical and tribological properties of self-lubricant W-S-N coatings, Surf. Coat. Technol. 261 (2015) 7–14, https://doi.org/10.1016/j.surfcoat.2014.11.074.
[73] T.W. Scharf, A. Rajendran, R. Banerjee, F. Sequeda, Growth, structure and friction behavior of titanium doped tungsten disulphide (Ti-WS_2) nanocomposite thin films, Thin Solid Films 517 (2009) 5666–5675, https://doi.org/10.1016/j.tsf.2009.02.103.
[74] B. Deepthi, H.C. Barshilia, K.S. Rajam, M.S. Konchady, D.M. Pai, J. Sankar, Mechanical and tribological properties of sputter deposited nanostructured Cr-WS_2 solid lubricant coatings, Surf. Coat. Technol. 205 (2010) 1937–1946, https://doi.org/10.1016/j.surfcoat.2010.08.074.
[75] X.H. Zheng, J.P. Tu, D.M. Lai, S.M. Peng, B. Gu, S.B. Hu, Microstructure and tribological behavior of WS_2-Ag composite films deposited by RF magnetron sputtering, Thin Solid Films 516 (2008) 5404–5408, https://doi.org/10.1016/j.tsf.2007.07.102.
[76] V.Y. Fominski, R.I. Romanov, A.V. Gusarov, J.P. Celis, Pulsed laser deposition of antifriction thin-film $MoSe_x$ coatings at the different vacuum conditions, Surf. Coat. Technol. 201 (2007) 7813–7821, https://doi.org/10.1016/j.surfcoat.2007.03.006.
[77] T. Polcar, M. Evaristo, M. Stueber, A. Cavaleiro, Synthesis and structural properties of Mo-Se-C sputtered coatings, Surf. Coat. Technol. 202 (2008) 2418–2422, https://doi.org/10.1016/j.surfcoat.2007.08.019.
[78] S.H. Mukhtar, M.F. Wani, R. Sehgal, M.D. Sharma, Nano-mechanical and nano-tribological characterisation of self-lubricating MoS_2 nano-structured coating for space applications, Tribol. Int. 178 (2023), https://doi.org/10.1016/j.triboint.2022.108017.
[79] P. Ying, H. Sun, P. Zhang, C. Lin, T. Yang, J. Wu, M. Huang, T. Wang, Z. Lian, V. Levchenko, Preparation and tribological properties of WS_2 solid lubricating coating with dense structure using HiPIMS, J. Mater. Res. Technol. 32 (2024) 530–540, https://doi.org/10.1016/j.jmrt.2024.07.214.
[80] T.A. Mufti, S.G. Jan, M.F. Wani, R. Sehgal, Development, mechanical characterization and high temperature tribological evaluation of magnetron sputtered novel MoS_2-CaF_2-Ag coating for aerospace applications, Tribol. Int. 182 (2023), https://doi.org/10.1016/j.triboint.2023.108374.